Full Title

MgO(111) Nanocatalyst for Biomass Conversion: A study of Carbon Coating Effects on Catalyst Faceting and Performance

Running Head

MgO(111) Nanocatalyst for Biomass Conversion

Author List

Raiven I. Balderas^{1,2}

Email: raivenbalderas@mines.edu
ORCID ID: 0000-0002-2659-675X

Amy E. Settle^{1,2,6}

Email: amy.settlemaurer@gmail.com

Allyson York^{1,2}

Email: allieyork@gmail.com

Davis R. Conklin²

Email: davis.conklin@gmail.com

Hien N. Pham³

Email: hipham@unm.edu

Peter C. Metz⁴

Email: metzpc@ornl.gov

Katharine Page⁵

Email: kpagr10@utk.edu

Abhaya K. Datye³

Email: datye@unm.edu

ORCID ID: 0000-0002-7126-8659

Brian G. Trewyn^{1,2}

Email: btrewyn@mines.edu

Derek R. Vardon^{1,2}

Email: derek.vardon@nrel.gov
ORCID ID: 0000-0002-0199-4524

Ryan M. Richards^{1,2}

Email: rrichard@mines.edu

Affiliations

¹Department of Chemistry, Colorado School of Mines, Golden, CO 80401, USA

²National Bioenergy Center, National Renewable Energy Laboratory, Golden, CO 80401, USA.

³Department of Chemical and Biological Engineering and Center for Microengineered Materials, University of New Mexico, Albuquerque, NM 87131, USA.

⁴Neutron Scattering Division, Oak Ridge National Laboratory, Oak Ridge, TN 37831, USA.

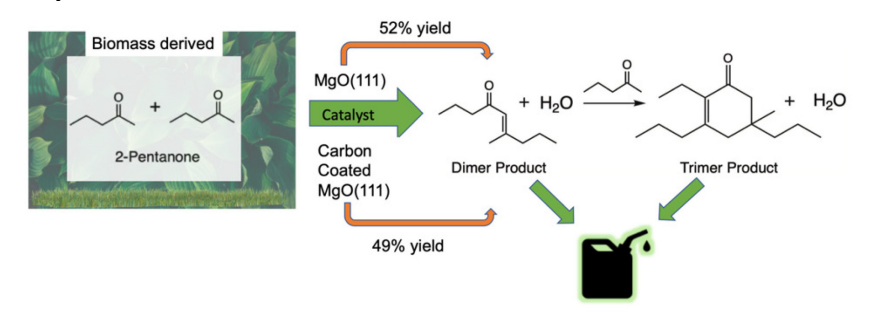
⁵Materials Science and Engineering Department, University of Tennessee, Knoxville, TN 37996, USA.

⁶Department of Physical and Environmental Sciences, Colorado Mesa University, Grand Junction, CO 80401, USA.

Abstract

Solid base metal oxide catalysts such as MgO offer utility in a wide variety of syntheses from pharmaceuticals to fuels. The (111) facet of MgO shows enhanced, unique properties relative to the other facets. Carbon coatings have emerged as a promising modification to impart metal oxide catalyst stability. Here, we report the synthesis, characterization, and catalytic properties of commercial MgO, MgO(111), and carbon coated derivatives thereof for 2-pentanone condensation. Our findings highlight the catalytic efficacy of MgO(111), provide insight into carbon coating for catalyst stability, and pave the way for continued mechanistic investigations.

Graphical Abstract



Keywords

Carbon coating; metal oxide; MgO; condensation; catalysis; faceting.

Introduction

Owing to natural abundance, facile synthesis, mechanical robustness, and tunable activity, metal oxides have been used as heterogenous catalysts since the mid-1950s for a myriad of applications.[1] Predominately, metal oxides are employed to catalyze acid-base or oxidation reactions, though they have been used for industrial processes such as environmental remediation, biomass conversion, and photocatalysis.[1-3] Recently, thin carbon coatings have emerged as a promising method to enhance the stability of metal oxide catalyst supports. For example, Pd and Cu nanoparticles supported on carbon coated Al₂O₃ and SiO₂ have demonstrated retention of structural integrity and catalytic activity of the intercalated metal nanoparticles before and after hydrothermal treatment.[4, 5]

Although carbon coatings have been investigated for metal oxide-supported catalysts, there is a dearth of information regarding their application for enhanced durability of metal oxides when the metal oxide itself is acting as the catalyst, and there is even less knowledge on the effects carbon coatings have on the faceting of metal oxide catalysts beneath the carbon coating. Over the years, advanced synthetic strategies have emerged for size and shape-controlled nanoparticles as well as methods to instigate the

preferential growth of targeted surface facets. With these new design strategies arises a whole new realm of facet dependent catalytic properties to be discovered and explored. Previous studies have highlighted the enhanced catalytic activity of MgO(111) versus commercial MgO, which has primarily (100) facets and is not facet controlled. For example, in the transesterification of vegetable oils toward biodiesel products, MgO(111) exhibits higher conversion and higher biodiesel yield than commercially available MgO or high surface area MgO, indicating that the (111) facet plays a significant role in dictating substrate interactions with the surface of the catalyst.[6] Even more recently, was the study of MgO(111) when exposed to water during 2-pentanone condensation, showing that the (111) facet is more active for ketone condensation than the (100) facet.[7] Additionally, when MgO(111) is used in the Claisen-Schmidt condensation of benzaldehyde, complete conversion is achieved in 10% of the amount of time it takes using commercial MgO.[2] The (111) surface of MgO consists of monolayers of cations (Mg²⁺) followed by a monolayer of oxygen and terminated by hydroxyl groups.[8]

Regarding the addition of a carbon coating, several fundamental questions arise regarding (i) the ability of carbon coated metal

oxides to allow the oxide to retain its innate catalytic behavior, (ii) the effects of carbon coatings on the physiochemical properties of metal oxide surfaces, and (iii) the extent to which metal oxide faceting plays a role in the catalytic activity and inherent characteristics. To address these knowledge gaps, this work examines the synthesis, characterization, and catalytic activity of carbon coated derivatives of MgO with different surface facets. We studied the condensation of 2-pentanone, a model methyl ketone for condensation studies. The reaction has industrial and sustainable relevance as methyl ketones can be biomass-derived and converted into both dimer and trimer products, the former of which resembles precursors suitable for diesel and the latter of which resembles common jet fuel molecules upon oxygen removal.[3, 9] The schematic for this reaction is shown in **Figure 1**. Batch reactor condensation reactions were used to screen the activity of uncoated and carbon coated catalysts, including commercially available MgO (denoted as "CM-MgO"), MgO(111), and hydrotalcite (a low-cost model catalyst for methyl ketone condensation denoted as "HTC"). The catalysts were extensively characterized to evaluate the impacts of carbon coatings on material properties including basicity, surface area, morphology, atomic structure, and catalytic activity.

Experimental

Catalyst Preparation

MgO(111) was synthesized as per the methods outlined in our previous work.[10, 11] To summarize, 1 g of magnesium ribbon was sanded, cleaned with acetone, and cut into strips approximately 2 cm long. The magnesium strips were added to a 500 mL three neck round bottom flask, purged with nitrogen for 15 min, and maintained under a nitrogen atmosphere. Subsequently, 120 mL of methanol was added to the flask and stirred at 300 rpm with continuous nitrogen flow. After 1 h, 4-methoxybenzylalcohol was added in a 1:2 molar ratio of 4-methoxybenzylacohol to magnesium and stirred for 5 h. Nanopure water (18.2 M Ω -cm) in a 2:1 molar ratio of water to magnesium with 40 mL of methanol was then added dropwise to the flask. After slow titration was completed, the nitrogen flow was shut off and the solution left to stir for 12-16 h. The solution was then transferred to a guartz-lined 600 mL Parr reactor and purged numerous times with argon. After purging, the reactor was pressurized with 5 bar argon, heated at 265°C at a ramp rate of 10°C/min, and held for 8 to 12 h. The reactor was vented while at 265°C and allowed to cool overnight. The resultant MgO hydrate powder was then calcined at 500°C for 6 hours at a ramp rate of 2.5°C/min to yield MgO(111) nanosheets.

MgO(111), CM-MgO (Sigma Aldrich, >99.99%), and HTC (Sigma Aldrich, magnesium aluminum hydroxycarbonate) were pretreated via calcination at 400°C for 3 h in a muffle furnace at a ramp rate of 3°C/min before characterization and reaction testing.

Carbon Coating of MgO and HTC Catalysts.

Similar to a previously reported method that results in the formation of a graphitic carbon coating, 3.0 g of MgO(111) was coated with carbon by dissolving 0.4013 g of 2,-3-dihydroxynaphthalene in 75 mL acetone.[12] MgO(111) was added to the solution and stirred for 24 h, permitting solvent evaporation. The resulting solid was pyrolyzed in a tube furnace under 100 sccm nitrogen and heated to 300°C at a ramp rate of 5°C/min, held for 1 h, heated to 800°C at a ramp rate of 5°C/min, held for 4 h, and cooled to room temperature. The solids were then collected and lightly ground with a mortar and pestle into a fine powder.

The same procedure was used for HTC and CM-MgO but was scaled down to use 0.5 g of catalyst for coating instead of 3.0 g. Carbon coated catalysts are denoted as "CC-MgO(111)", "CC-CM-MgO", and "CC-HTC". All samples were pre-treated via calcination at 400°C for 3 h in a muffle furnace at a ramp rate of 3°C/min before characterization and reaction testing.

Characterization and Catalytic Testing.

BET Surface Area.

Nitrogen physisorption analysis was conducted on a Micromeritics ASAP 2020 instrument using a 55-point nitrogen adsorption/desorption curve at 77 K. Prior to analysis, samples were degassed under vacuum at 300°C at a ramp rate of 10° C/min and held for 5 h. Data for BET surface areas were collected over a relative pressure range of 0.060 to 0.200 P/P₀.

Determination of Base Sites via Chemisorption.

Base site quantification was performed via CO₂ temperature programmed desorption (TPD) using an AutoChem II 2920 chemisorption instrument. The sample was loaded into a "u" shaped quartz tube lightly packed with quartz wool and 30 mg of sample. The sample was pre-treated *in situ* under flowing helium while heating to 350°C and held for 2 h. The sample was cooled to 40°C upon which it was dosed with 10% CO₂ (balanced with helium) for 90 min, and subsequently purged with helium for 60 min. For temperature desorption studies, the sample was heated to 450°C under flowing helium and was allowed to cool to room temperature. Measurements were recorded at a rate of one data point per second for pretreatment and dosing experiments. Evolved CO₂ was quantified by a calibrated thermal conductivity

detector. All flow rates were 50 sccm, and temperature was ramped at 10°C/min at each heating and cooling step.

Nitrogen DRIFTS.

Diffuse reflectance Fourier transform infrared spectroscopy (DRIFTS) spectra were taken using a Thermo 6700 FT-IR spectrometer with a Smart Accessory DRIFTS attachment. The sample was loaded into the cell and purged with UHP nitrogen at 30 sccm for 10 min. Spectra represent the average of 32 scans with a resolution of 4 cm⁻¹. The spectra were each referenced to a potassium bromide background that was collected using the same method.

Carbon Content Analysis via Thermogravimetric Analysis (TGA).

TGA data were collected using a TGA Q50 (TA Instruments) by loading 10 mg of sample into a ceramic pan and heating to 120°C, holding for 30 min, followed by heating to 550°C and holding for 1 h. The sample was continuously exposed to 60% house air and 40% nitrogen flow at 50 sccm, and each ramp rate was 10°C/min. After holding for 1 h the sample was allowed to cool to room temperature. Carbon content was determined by subtracting the small mass loss due to water from the total mass loss experienced by each sample.

High-Resolution Transmission Electron Microscopy (HRTEM).

To image the carbon layers on MgO(111), samples were dispersed in ethanol and mounted on holey carbon grids for examination in a JEOL NeoARM 200CF transmission electron microscope equipped with spherical aberration correction to allow atomic resolution imaging. Images were recorded in bright field mode.

Batch Reaction Screening.

Batch reactor products were analyzed by gas chromatographyflame ionization detector/mass spectrometry (GC-FID/MS) using an Agilent 7890A GC equipped with a 5973 MS (Agilent Technologies) operating in split mode (25:1). The GC was equipped with an Agilent HP-5ms column (30 m × 0.25-mm ID, 0.25-µm film), and helium (1.4 sccm column flow) was used as the carrier gas at 1 sccm. The injector volume was set to 1 µL using an Agilent autosampler. The GC-MS method consisted of a front inlet temperature of 260°C, and an MS transfer line temperature of 260°C. A starting temperature of 40°C was held for 2 min and then ramped at 18°C/min to a temperature of 280°C and held for 5 min before cooling. Samples were analyzed simultaneously Polyarc®system/FID and MS. The FID was set at 300°C, helium flow at 30 sccm, air flow at 350 sccm, and makeup flow at sccm. The MS transfer line temperature was set at 293°C. The trimer product of 2-pentanone condensation was directly quantified using an analytical standard. The dimer product quantities were estimated using the difference between trimer and total product (e.g., stock solution - (2-pentanone remaining + trimer) = dimer).

High resolution mass spectra were collected using a JEOL GCmate II double-focusing mass spectrometer (JEOL, Peabody, MA) coupled with a DSC/TGA Q600 (TA Instruments, Newcastle, DE). Liquid samples were introduced to the MS via a heated transfer line and evaporated by heating in the DSC/TGA instrument to their boiling point. Calorimetric data were not collected as the aim of these experiments were to collect mass spectra of volatilized compounds only. The ionization source was operated in the electron ionization (EI) mode at 70 eV. The MS was tuned prior to experiments to a resolving power of \geq 6,000 (full width at half maximum (FWHM)) based on m/z 69 using the spectrum of perfluorokerosene. The full spectrum of perfluorokerosene was used for mass calibration across the range of the spectrum collected from m/z 35 to 400.

Control Tests.

Control tests were performed using uncoated MgO(111) to determine if leached metal oxide was partially responsible for the observed catalytic activity. Into each 20 ml Pyrex tube, 20 mg

catalyst, 20 μ L 2-pentanone, and 4 mL of toluene were added. The reaction vessels were heated to 140°C for 5 h, and then cooled to room temperature. The catalyst was filtered out and liquid product was subsampled. The reaction was then reheated to 140°C for an additional 5 h at 140°C before cooling and analyzing the liquid products. Control tests were also performed with carbon coated silica to determine if the carbon coating itself was responsible for any observed activity using the same reaction conditions listed above.

Normalization of Turnover Number.

The initial turnover number (TON) was determined for each catalyst by calculating the moles of 2-pentanone converted per µmol of base sites per m² of surface area at 30 min of reaction time. Surface area was incorporated in the normalization calculation due to the variance in surface area between CM-MgO, MgO(111), and HTC; the surface area of CM-MgO being eight times lower than that of MgO(111) and HTC.

Neutron Total Scattering.

Neutron powder diffraction and neutron pair distribution function (NPDF) data were acquired using the Nanoscale Ordered Materials Diffractometer (NOMAD) at the Spallation Neutron Source (SNS, Oak Ridge National Laboratory).[13] Samples were

measured in sealed vanadium cans at 300 K. Post-processing of the raw neutron time-of-flight data was performed using the Advanced Diffraction Environment (*ADDIE*), including pixel calibration, intensity normalization, and container subtraction.[14] Pair distribution function (PDF) data were also reduced using *ADDIE*, with maximum momentum transfer $Q = 31.4 \, \text{Å}^{-1}$.

Rietveld refinement of data from the three higher resolution banks of NOMAD ($\Delta d/d \approx 0.004\text{-}0.013$) was performed using *TOPAS-Academic* v.6.[15] The instrumental peak shape was described by convolution of a symmetric pseudo Voigt profile and an asymmetric back-to-back exponential characteristic of the incident beam moderator. The instrumental profile parameters were optimized against NIST SRM 640d (Si) data collected in a similar experimental configuration.[16] NPDF refinements were performed using *PDFgui*.[17] The parameters describing the influence of instrumental resolution on the PDF data were again fixed according to refinement of standard Si data.[18]

Results and Discussion

To confirm the faceting of MgO(111), HRTEM was used in conjunction with DRIFTS. Although there are other particles with exposed MgO(200) surfaces, the needle-like MgO particles have exposed (111) surfaces shown in **Figure 2A**. The yellow box shown

in the HRTEM image (**Figure 2B**) is where the FFT pattern was obtained. The diffraction spots are shown in the FFT pattern (**Figure 2C**), with emphasis on the d-spacing of 0.243 nm corresponding to the (111) lattice planes for MgO.[10] The region in the white circle shows (111) lattice fringes, and they run along the length of the MgO particle. The peak at 3763 cm⁻¹ in the DRIFTS spectrum supports this claim (**Figure 2D**), as it indicates the presence of 3-coordinate hydroxyl groups, corresponding to an undercoordinated surface, which is characteristic of a (111) surface.[19]

To evaluate the structural influence of carbon coatings on the catalyst structure, carefully selected characterization methods were utilized. Since previous work shows that graphitic carbon is stable under harsh conditions, Raman spectra were collected to investigate the graphitic nature of the 10 wt.% carbon coated catalysts.[12] Raman spectroscopy is commonly used as a simple technique to identify the ratio of "disordered" carbon to graphitic carbon. The "disordered" peak, or "D" peak, can be found at around 1340 cm⁻¹ and the graphitic, or "G" peak, is around 1580 cm⁻¹.[20] If the ratio of D/G peak intensities is around 1, the material is considered graphitic.[21, 22] **Figure 3** depicts the Raman spectra that were collected for all three carbon coated catalysts.

The intensities for the D and G peaks for each spectrum are listed in **Table 1**, along with the D/G peak intensity ratio. Although the resolution of these peaks is not as clear for MgO(111) or HTC as it is for CM-MgO, the observed intensities at each Raman shift indicate that the carbon coating on each material is graphitic, as the D/G ratios are all at or near 1. Neutron scattering data collected on the same materials, discussed in greater detail below, also indicates the presence of a graphite-like bonding motif with nanoscale coherence.

The HRTEM images in **Figure 4** of 10 wt.% CC-MgO(111) illustrate that the carbon coatings do not alter the structural integrity of the catalyst, with well-defined lattice fringes and sheet-like nature of the MgO(111) nanosheets retained after carbon coating. **Figures 4A-C** show MgO coated with a thin layer of carbon as indicated by the yellow arrows. The red box shown in **Figure 4C** is where the FFT pattern was obtained and the region in the white circle shows (111) lattice fringes, and they run along the length of the MgO nanoparticle. The diffraction spots in the FFT pattern in **Figure 4D**, as indicated by yellow arrows, are the (111) planes. The carbon coating does not alter the morphology of the MgO(111) nanoparticles. Electron microscopy and Raman scattering were corroborated using neutron total scattering measurements. Bulk

MgO(100) particles and MgO(111) oriented tabular nanoparticles with 0, 10, and 30 wt.% carbon coating were studied using mediumresolution neutron powder diffraction and neutron pair distribution function (NPDF) analysis. NPDF data was acquired due to its capability to reveal local atomic structure for disordered crystalline materials, nanomaterials, and amorphous materials as well as its sensitivities to light atom species. The phase purity and approximate coherent scattering domain size of the MgO were investigated using bank-by-bank Rietveld refinement of the integrated neutron powder diffraction data. MgO crystallizes in the Fm-3m space group with Mg and O occupying the 4a and 4b Wyckoff positions at (0, 0, 0) and $(\frac{1}{2}, \frac{1}{2}, \frac{1}{2})$, respectively. The cubic lattice parameter a and the isotropic atomic displacement parameters $B_{iso} = 8\pi^2 \langle u^2 \rangle$ were refined. Isotropic crystallite size broadening was refined using a Lorentzian peak profile model (denoted CS-L). The fitted parameters are tabulated in **Table 2**.

Data from NOMAD bank 2 and the corresponding refinement result is shown in **Figure 5**. The location of the graphite (002) reflection is also noted. The bulk MgO(100) powder was demonstrated to be phase pure, with crystallite domain size sufficiently large as to be indistinguishable from the instrumental background. The MgO(111) nanopowder was well-fit by the same

model, though with substantially size-broadened Bragg Peaks. Carbon coated MgO(111) nanopowders were generally well-fit using a single MgO phase, although missing diffuse intensity (best observed in the shape of the green difference curves in **Figure 5**) becomes increasingly noticeable, particularly in the 30 wt.% carbon coated sample. This, and the fact that the graphite (002) reflection was all but absent throughout the compositional range indicates the absence of bulk carbon that has phase segregated, suggesting that the carbon coating is nanostructured, disordered, and only present on the surface of the MgO.

The refined lattice parameters and atom displacement parameters of the MgO(111) nanopowders were slightly larger than the values refined for the bulk MgO(100) powder, indicating the lattice is very slightly relaxed in the nanostructured variant. The isotropic size broadening model, despite neglecting the possibly anisotropic crystallite shape known *a priori* from HRTEM imaging, implies an average crystallite size on the order of 10 nm which is in good agreement with the ~5 nm particle size estimated by microscopy.

To gain further insight into the structure of the carbon coating, NPDF data were fit over 1-25 Å using PDFgui and the standard MgO model described above.[17] In the case of the MgO(111) data, a

spherical analytic shape function was applied to approximate the shape envelope of the nanoparticle (Supplemental information Figure S1).[23] A graphitic carbon model was introduced to account for the nanostructured carbon correlations at low-r, with a 6 Å cutoff determined by inspection of single-phase fits (Supplemental Information Figure S2). The carbon phase was modelled as P6₃/mmc graphite with carbons occupying the 2b and 2c Wyckoff positions. The a=b lattice parameter, which determines the nearest-neighbor carbon distance, was refined, while the c-lattice parameter which determines the interlayer spacing was fixed. Atomic displacement parameters were treated as isotropic in the case of the MgO phase, while the carbon model was assigned independent U₁₁=U₂₂ and U₃₃ parameters to approximate loss of coherence between adjacent graphene layers in a disordered graphite. For brevity, the resulting fit and component PDFs of 30 wt.% CC-MgO(111) sample are presented in Figure 6; the results for the 10 wt.% and 0 wt.% carbon coating samples differ only in relative amplitude of the constituent signals. The refined parameters are tabulated in **Table 3**.

Consistent with the Rietveld analysis, the PDF-refined atomic displacement parameters are slightly larger in the nanoscale MgO(111) powders as compared with the bulk MgO(100) sample.

Additionally, the oriented MgO(111) has a significantly attenuated PDF, consistent with the smaller refined spherical diameter (ca. 5-6 nm). Otherwise, the data are well described by a mechanical mixture of MgO and graphite, implying there is a limited degree of correlation between the carbon and MgO domains. The small degree of misfit observed in the low-r region of the PDF (**Figure 6**) could be attributed either to C-Mg and C-O correlations not represented in this model, or to amorphization of the carbon phase yielding irregular relative C-C correlation amplitudes.

The neutron scattering data thus infer that the parent nanoparticle MgO structure is largely unchanged from that of the bulk, with slightly larger atomic displacement parameter values indicating perhaps slight lattice relaxation of the nanoparticle. The carbon phase exists as a severely disordered phase with coherent graphite-like domains smaller than 1 nm. The minor fit residual in this simple two-phase model implies that an epitaxial relationship between the carbon and MgO domains is unlikely. This doesn't necessarily rule out an intimate contact between the carbon and MgO as seen in **Figure 4** showing the MgO(111) nanoparticles are clearly coated by carbon and is not a physical mixture since carbon is not shown as being separated from MgO, but implies the carbon is either not strongly bonded to the MgO (in which case we would

anticipate at least one clear bond length) or the contact is not ordered in any fashion.

Physiochemical Surface Characteristics.

To assess the physiochemical properties of the catalysts with 10 wt.% carbon coating, BET surface areas and the base site densities were evaluated before and after coating, values for which can found in Table 4. BET surface areas of CM-MgO and MgO(111) before and after coating were relatively unchanged, but HTC exhibited a significant decrease in surface area. This could indicate a difference in the chemical transformation that occurred on the surface when the carbon precursor was pyrolyzed.[24] Base site counts obtained via CO₂ TPD indicate that the number of base sites decrease for all three catalysts perhaps due to the carbon coating partially blocking the sites (as depicted in **Table 4** and **Figure 7**). CC-CM-MgO and CC-HTC both experienced a significant reduction in base site counts while CC-MgO(111) experienced only a slight reduction. This demonstrates that the carbon coating process permits CO₂ to interact with the base sites of the carbon coated catalysts in a similar manner of interaction as with the base sites of the uncoated MgO(111). It is inferred that the carbon coating similarly impacts the ability of 2-pentanone to access the active sites of the metal oxides, though elucidation of the mechanism by

which 2-pentanone interacts with active sites through the carbon coating will be the subject of future work.

CO₂ TPD profiles provide insight not only into base site quantity, but also strength. Figure 7 depicts these profiles for uncoated and carbon coated catalysts. The trend of each profile remains the same among each catalyst's uncoated and carbon coated counterparts, indicating that the carbon coating is not altering the integrity of the basicity of each material. It also highlights that CM-MgO has very low CO₂ adsorption and desorption when compared to MgO(111) and HTC. The primary peak for CM-MgO occurs near 100°C and could be due to a low-strength CO₂ binding site. There is a slight shoulder present in this temperature range for MgO(111) and HTC, but each of their primary peaks occur near 150°C signifying that these are stronger base sites than the ones present in CM-MgO. Furthermore, MgO(111) has an additional peak around 280°C, indicating stronger base sites than HTC. Overall, the characterization of the catalysts before and after carbon coating suggests that the physiochemical properties of MgO(111) are slightly affected whereas CM-MgO and HTC experience significant changes.

2-Pentanone Condensation Reaction.

CM-MgO, MgO(111), and HTC were tested for activity toward 2-pentanone condensation before and after applying a 10 wt.% carbon coating. The degree of conversion and product distribution of each catalyst was evaluated at 0.5, 1, 1.5, and 2 h of reaction at 140°C. Pre-normalized data is found in **Figure 8**.

The time series in **Figure 8** shows that CM-MgO has low 2-pentanone conversion and product yield independent of whether it has a carbon coating or not. MgO(111) exhibits moderate 2-pentanone conversion when uncoated and when carbon coated (64% and 53% conversion at t=2 h, respectively). HTC exhibits the highest 2-pentanone conversion whether it is uncoated or carbon coated (93% and 56% conversion at t=2 h, respectively). These percentages indicate that the carbon coating is drastically affecting the catalytic performance of HTC while MgO(111) is the least affected. As the reaction progresses, comparable dimer and trimer yields between uncoated and carbon coated MgO(111) and HTC can be seen in **Figures 8B,E** and **Figures 8C,F** respectively, albeit with differing selectivities and product distribution between the two catalysts.

As seen in previous studies, HTC has a high selectivity towards trimer formation and this is confirmed in **Figure 8C**.[9] Meanwhile MgO(111) displays a higher selectivity towards dimer formation

shown in **Figures 8B,E**. MgO(111) experiences slight decreases in dimer production from 52% to 49% as well as trimer production from 12% to 4% upon carbon coating. Despite HTC showing the highest conversation rates before and after coating, the catalyst experiences a drastic decrease in trimer production from 54% to 11%; however, dimer production increases slightly from 39% to 45% upon carbon coating. The difference in 2-pentanone conversion, dimer, and trimer production for all three catalysts upon carbon coating can be seen in **Table 5**. This data shows how MgO(111)'s selectivity to dimer products is only minimally affected, whereas HTC's selectivity to trimer product is drastically affected.

The results highlight the higher catalytic activity of MgO(111) versus CM-MgO which predominately contains (100) facets. Although they are of the same chemical composition, the controlled (111) faceting positively impacts the 2-pentanone conversion into dimer products. After assessing catalytic activity of the uncoated-vs. carbon coated catalysts, control tests on uncoated and carbon coated SiO₂ and MgO(111) were conducted to confirm that-neither the carbon coating itself nor active site leaching is responsible for the observed activity retention (Supplemental Information **Table S1**).

Figure S3 depicts the TON at t=30 min of the carbon coated and uncoated catalysts, normalized to mmol base sites per m² catalyst surface area. In agreement with batch reaction time series shown in Figure 8, carbon coated and uncoated CM-MgO displayed the lowest TON, while uncoated HTC displayed the highest TON. All three catalysts experienced a decrease in TON upon carbon coating. This is expected because the carbon coating may obstruct the interaction between 2-pentanone and the active surface of the catalysts as witnessed by the base site counts decreasing for all three catalysts from CO₂ TPD studies.

The catalytic data thus infers that the reaction could be occurring on the exposed active sites remaining after carbon coating. Because the carbon coating is inferred to be nonepitaxial and disordered from the neutron total scattering studies, this may provide a reason as to how these active sites are still accessible upon carbon coating and catalytic activity is retained.

Conclusions

The structure and catalytic performance of commercial bulk MgO with exposed (100) surfaces and nanoparticle MgO with exposed (111) surfaces with 0, 10, and 30 wt.% carbon loadings have been thoroughly investigated. The parent nanoparticle of MgO(111) and CM-MgO(100) structures are largely unchanged after a carbon

coating process with slightly larger atomic displacement parameter values indicating relaxation of the nanoparticle lattice. NPDF reveals the carbon phase exists as a severely disordered phase with coherent graphite-like domains smaller than 1 nm. Successful modeling of the NPDF as a two-phase mixture implies no epitaxial relationship between the carbon and MgO domains formed and any contact between carbon and MgO is speculated to either not be strongly bonded or disordered.

When comparing MgO catalysts for 2-pentanone conversion, MgO(111) far exceeds CM-MgO in TON and selectivity when normalized to surface area, which reaffirms the positive influence of the (111) facet on catalytic activity. Upon carbon coating of the two MgO catalysts and a benchmark catalyst (HTC), all three catalysts exhibit a decrease in initial activity, however, MgO(111) experiences the least impact with regards to 2-pentanone conversion and selectivity to dimer formation. While trimers of methyl ketones can be used as jet fuel precursors, diesel precursors are mostly composed of linear structures and; therefore, would require stopping the reaction after dimerization.[9] MgO(111) displays a higher selectivity towards dimer formation before and after coating compared to CM-MgO and HTC and; therefore, is a

suitable catalyst in regards to facile synthesis, cost, and earth abundance for the preparation of dimer precursors for biofuels.

These results show that the carbon coating minimally impacts the catalytic performance of MgO(111). Control tests confirmed there was no leaching of the active phase and the carbon coating itself was not responsible for the observed activity. The carbon coating; therefore, retains the key active site structures needed to catalyze the 2-pentanone condensation reaction and thus is suitable to maintain catalytic stability for MgO(111). Further tests are needed to conclude whether the same effect is seen when carbon coated MgO(111) is subjected to hydrothermal treatments during 2-pentanone condensation since metal oxides are typically sensitive to water deactivation due to active site quenching and dissolution.[1-3, 25]

Acknowledgments

Neutron diffraction and PDF modeling was partially supported through the U.S Department of Energy (DOE), Office of Science, Office of Basic Energy Sciences, Early Career Research Program Award KC040602, under Contract DE-AC05-000R22725. A portion of this research used the NOMAD instrument at the Spallation Neutron Source, a DOE Office of Science User Facility operated by the Oak Ridge National Laboratory. The catalyst characterization

via TEM was supported by the DOE/BES Catalysis Science Program, grant DE-FG02-05ER15712. Acquisition of the electron microscope acquisition was supported by NSF grant DMR-1828731. RMR, DV, BGT, AY, and RIB also acknowledge the Colorado Energy Collaboratory for financial support.

References

- [1]. Vedrine JC (2017) Catalysts 7.
- [2]. Cadigan CA, Corpuz AR, Lin F, Caskey CM, Finch KBH, Wang X, Richards RM (2013) Catalysis Science & Technology 3:900-911.
- [3]. Sacia ER, Balakrishnan M, Deaner MH, Goulas KA, Toste FD, Bell AT (2015) Chemsuschem 8:1726-1736.
- [4]. Pham HN, Anderson AE, Johnson RL, Schmidt-Rohr K, Datye AK (2012) Angewandte Chemie-International Edition 51:13163-13167.
- [5]. Pham HN, Anderson AE, Johnson RL, Schwartz TJ, O'Neill BJ, Duan P, Schmidt-Rohr K, Dumesic JA, Datye AK (2015) Acs Catalysis 5:4546-4555.
- [6]. Verziu M, Cojocaru B, Hu JC, Richards R, Ciuculescu C, Filip P, Parvulescu VI (2008) Green Chemistry 10:373-381.
- [7]. Huo X, Conklin DR, Zhou M, Vorotnikov V, Assary RS, Purdy SC, Page K, Li Z, Unocic KA, Balderas RI, Richards RM, Vardon DR (2021) Applied Catalysis B: Environmental 294.
- [8]. Thomele D (2021) Crystal Growth & Design.
- [9]. Wu LP, Moteki T, Gokhale AA, Flaherty DW, Toste FD (2016) Chem 1:32-58.
- [10]. Zhu KK, Hu JC, Kubel C, Richards R (2006) Angewandte Chemie-International Edition 45:7277-7281.
- [11]. Hu JC, Zhu K, Chen LF, Kubel C, Richards R (2007) Journal of Physical Chemistry C 111:12038-12044.
- [12]. Duan P, Cao XY, Pham H, Datye A, Schmidt-Rohr K (2018) Materials 11.
- [13]. Neuefeind J, Feygenson M, Carruth J, Hoffmann R, Chipley KK (2012) Nuclear Instruments & Methods in Physics Research Section B-Beam Interactions with Materials and Atoms 287:68-75.
- [14]. McDonnell MT, Olds DP, Pagel KL, Neufeindl JC, Tucker MG, Bilheux JC, Zhou W, Peterson PF (2017) Acta Crystallographica a-Foundation and Advances 73:A377-A377.

- [15]. Coelho AA (2018) Journal of Applied Crystallography 51:210-218.
- [16]. Black DR, Windover D, Henins A, Gil D, Filliben J, Cline JP (2010) Powder Diffraction 25:187-190.
- [17]. Farrow CL, Juhas P, Liu JW, Bryndin D, Bozin ES, Bloch J, Proffen T, Billinge SJL (2007) Journal of Physics-Condensed Matter 19.
- [18]. Olds D, Saunders CN, Peters M, Proffen T, Neuefeinda J, Page K (2018) Acta Crystallographica a-Foundation and Advances 74:293-307.
- [19]. Mutch GA, Shulda S, McCue AJ, Menart MJ, Ciobanu CV, Ngo C, Anderson JA, Richards RM, Vega-Maza D (2018) Journal of the American Chemical Society 140:4736-4742.
- [20]. Hong J, Park MK, Lee EJ, Lee D, Hwang DS, Ryu S (2013) Scientific Reports 3.
- [21]. Pimenta MA, Dresselhaus G, Dresselhaus MS, Cancado LG, Jorio A, Saito R (2007) Physical Chemistry Chemical Physics 9:1276-1291.
- [22]. Liu L, Ryu SM, Tomasik MR, Stolyarova E, Jung N, Hybertsen MS, Steigerwald ML, Brus LE, Flynn GW (2008) Nano Letters 8:1965-1970.
- [23]. Kodama K, Iikubo S, Taguchi T, Shamoto S (2006) Acta Crystallographica Section A 62:444-453.
- [24]. Bartholomew CH (2001) Applied Catalysis a-General 212:17-60.
- [25]. Schwach P, Frandsen W, Willinger MG, Schlogl R, Trunschke A (2015) Journal of Catalysis 329:560-573.

Figures and Tables

Figure 1. Reaction Scheme for the condensation of 2-pentanone.

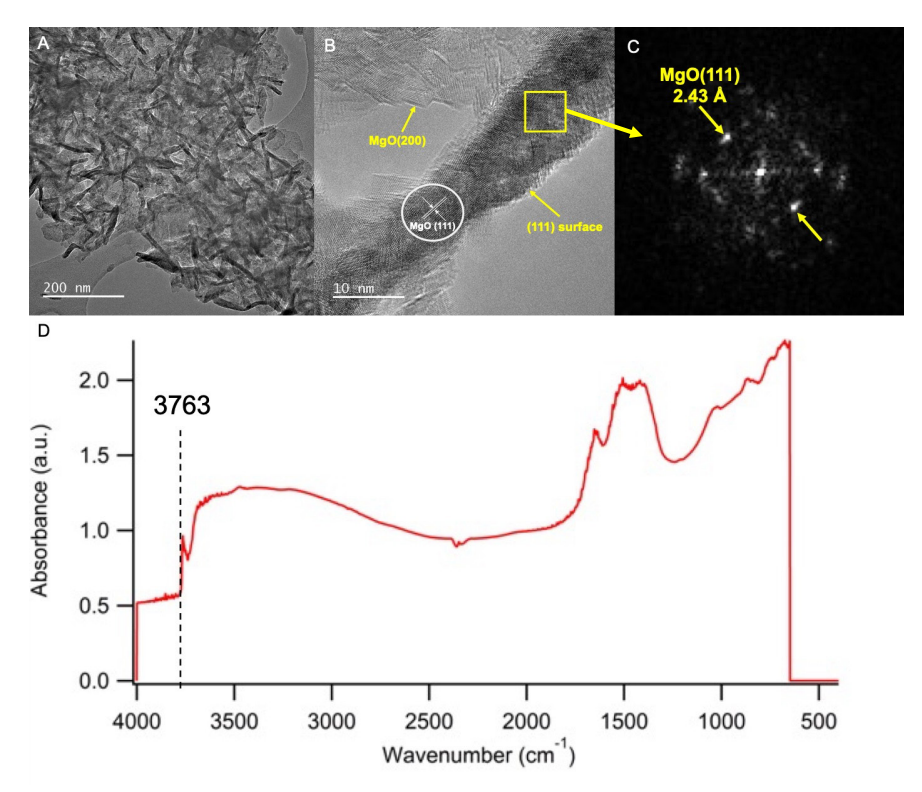


Figure 2. (A-B) Low resolution and HRTEM image of MgO(111), (C) faceting is confirmed by using FFT in HRTEM to measure d-spacings, and (D) N_2 DRIFTS to observe the 3-coordinate surface hydroxyl peak at 3763 cm⁻¹.

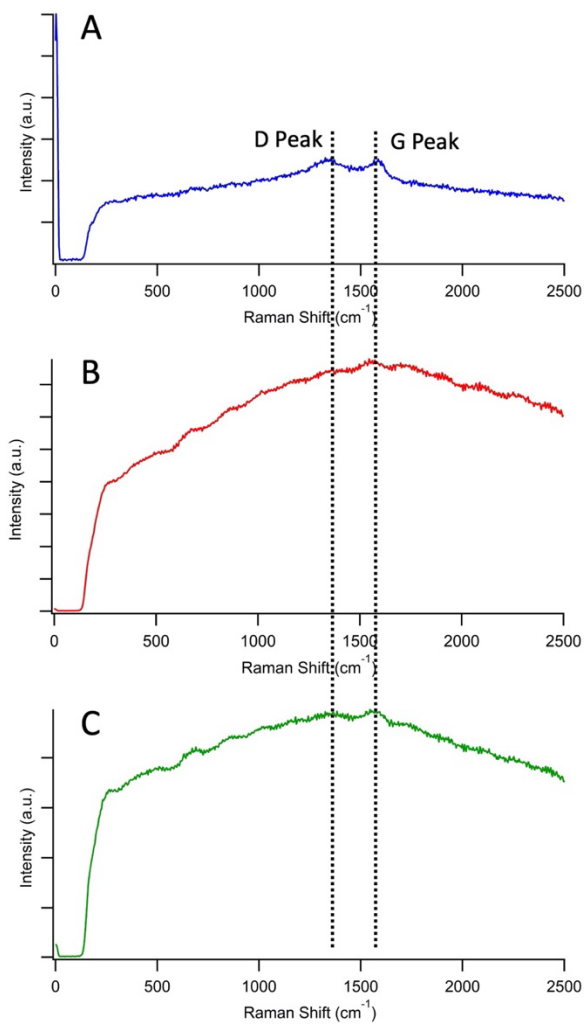


Figure 3. Raman Spectra of (A) CC-CM-MgO, (B) CC-MgO(111), and (C) CC-HTC. 10 wt.% coating.

Catalyst	D Peak		G Peak		D/G Ratio
	Shift (cm-1)	Intensity (a.u)	Shift (cm-1)	Intensity (a.u.)	
CC-CM-MgO	1329	251	1581	249	1.008
CC-MgO(1111)	1362	1686	1545	1757	0.960
CC-HTC	1383	696	1569	690	1.004

Table 1. Raman shifts, corresponding intensities, and D/G ratios for each 10 wt.% carbon coated catalyst.

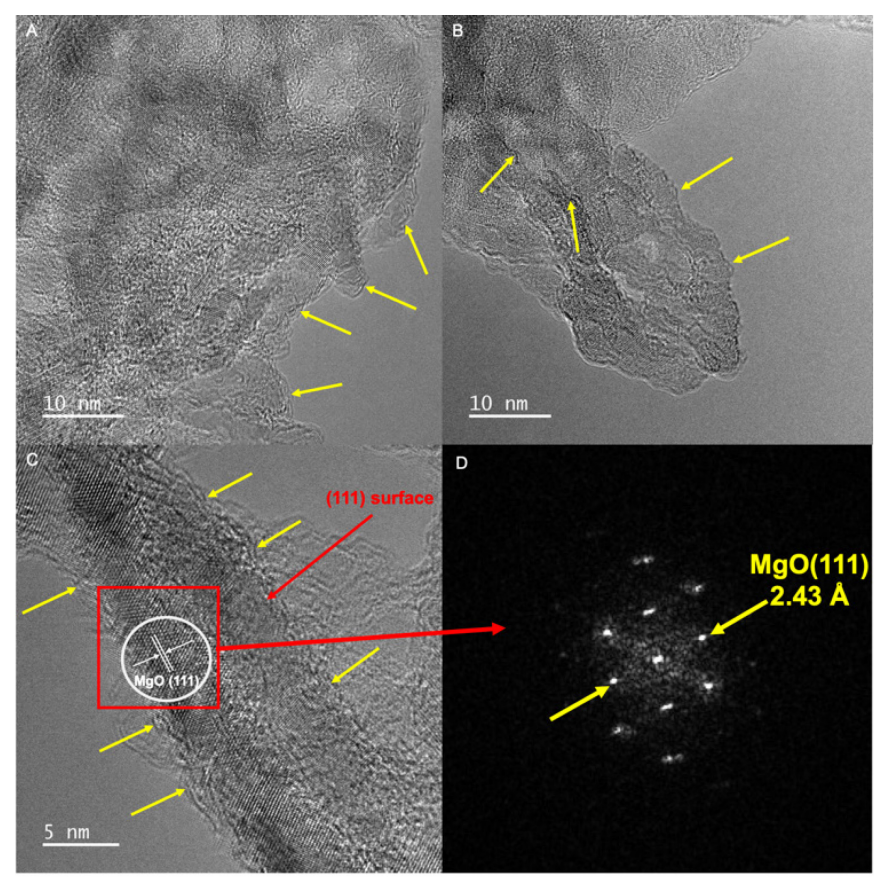


Figure 4. (A-B): HRTEM images of CC-MgO(111). Yellow arrows show the carbon coated layers. (C-D): HRTEM image and FFT respectively of CC-MgO(111). 10 wt.% carbon coating.

	(100)	(111)			
	0 wt.% C	0 wt.% C	10 wt.% C	30 wt.% C	
a [Å]	4.21301(3)	4.2226(1)	4.21987(9)	4.2209(1)	
CS-L [nm]	-	8.99(3)	11.21(3)	9.35(3)	
Uiso Mg [Å2]	0.00450(1)	0.0084(1)	0.0098(1)	0.0049(3)	
Uiso O [Å2]	0.0038(1)	0.0050(1)	0.00619(1)	0.0080(3)	
Rwp [%]	7.72	1.77	2.10	2.14	

Table 2. Rietveld Refined Parameters.

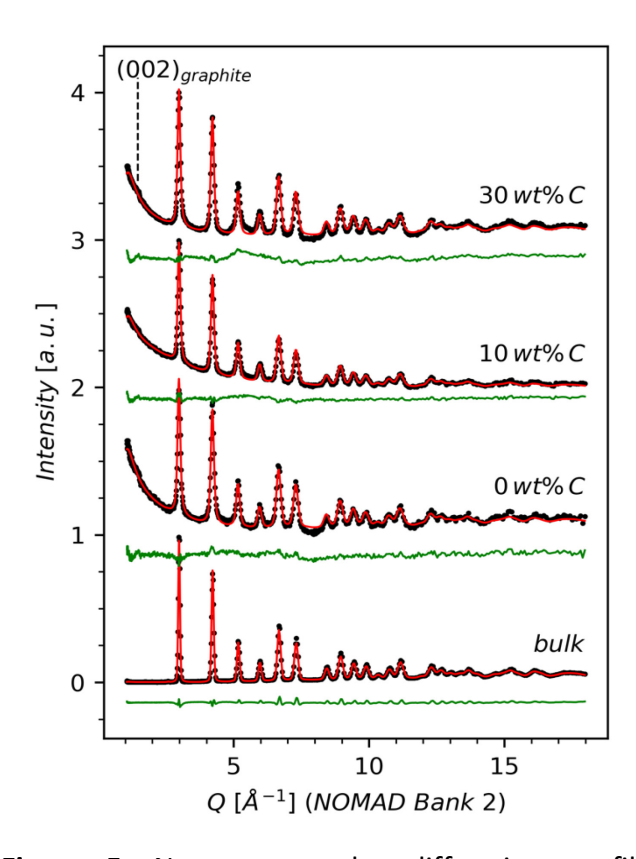


Figure 5. Neutron powder diffraction profiles and Rietveld refinement results for bulk MgO(100), nanopowder MgO(111), and carbon coated MgO(111).

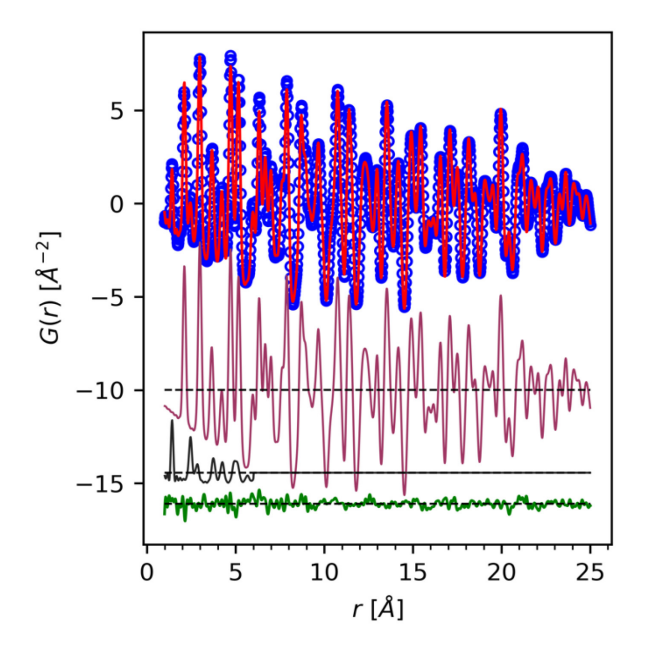


Figure 6. 2-phase fit of the 30 wt.% CC-MgO(111) neutron PDF data (blue o, red -) with MgO (plum -) and graphite (black -) contributions and fit residual (green -) offset (Rwp = 8.4%).

	(100)	(111)		
	0 wt.% C	0 wt.% C	10 wt.% C	30 wt.% C
	MgO			
a [Å]	4.2111(2)	4.220(2)	4.2181(8)	4.218(1)
scale	1.38(2)	0.38(3)	0.65(3)	0.40(3)
δ_1 [Å]	0.95(8)	1.1(3)	1.0(2)	1.1(3)
U _{iso} Mg [Å ²]	0.0045(4)	0.006(1)	0.006(1)	0.006(2)
U _{iso} O [Å ²]	0.0058(5)	0.009(2)	0.009(1)	0.008(2)
Sp. Dia. [Å]	216(31)	52(7)	67(7)	56(7)
	Graphite			
a [Å]	-	-	2.45(5)	2.45(3)
c [Å]	-	-	*8.6	*8.6
scale	-	-	0.10(5)	0.13(5)
δ_1 [Å]	-	-	1.2(3)	1.2(3)
U ₁₁ C [Å ²]	-	-	0.0111(9)	0.006(4)
U ₃₃ C [Å ²]	-	-	4.7(4.8)	3.9(3.3)
cut off [Å]	-	-	6.5	6.5
N _{varys} .	6	6	11	11
R _{wp} [%]	5.1	11.8	7.8	8.5
*Fixed				

 Table 3. 1- and 2-phase model PDFgui fitted parameters.

	Base Site Quantities (μmol g ⁻ 1)		Surface area (m ² g ⁻¹)	
Catalyst	Uncoated	Carbon	Uncoated	Carbon Coated
		Coated		
CM-MgO	85	45	25	22
MgO(111)	416	409	212	220
HTC	379	208	216	145

Table 4. Base site and active surface area of fresh catalysts with and without carbon coating. 10 wt.% carbon coating.

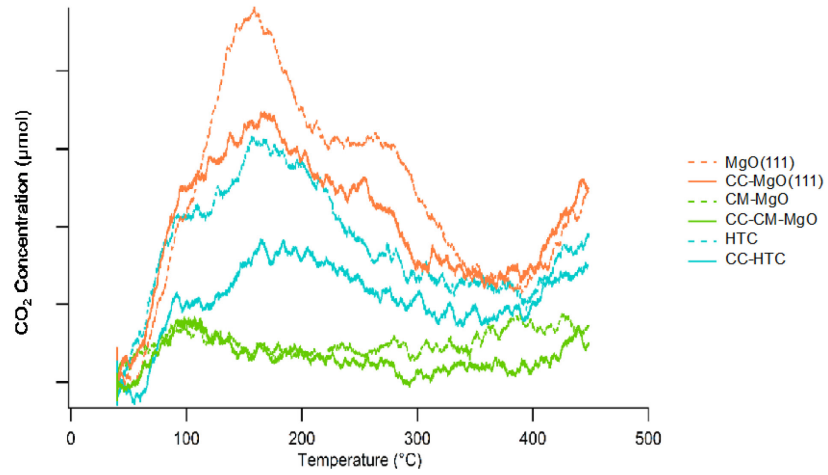


Figure 7. CO_2 TPD profile of uncoated and carbon coated MgO(111), CM-MgO, and HTC catalysts as a function of temperature and CO_2 concentration. 10 wt.% carbon coating.

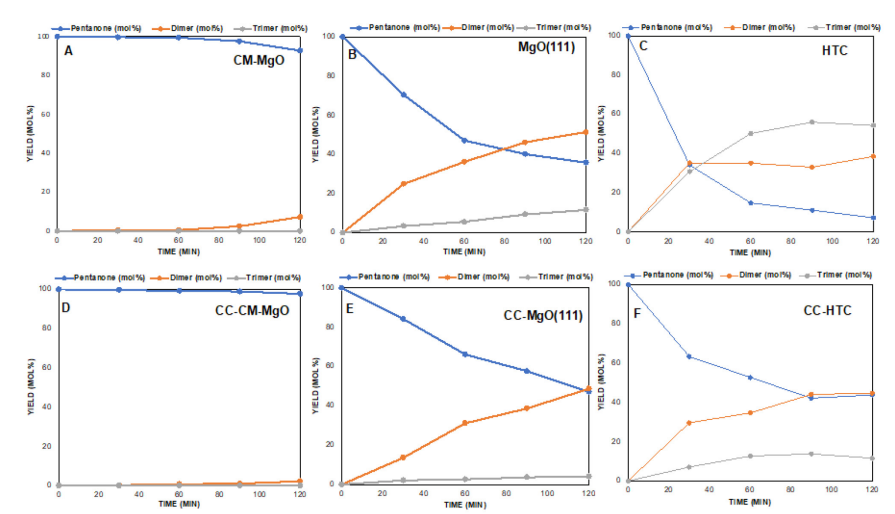


Figure 8. Pre-normalized time series data for all uncoated (A-C) and 10 wt.% coated catalysts (D-F) for the first 2 h of reaction progress. Reaction conditions: 50 mg catalyst, 50 mL 2-pentanone, 3 mL toluene, 150°C.

Catalyst	Δ 2-Pentanone (mol%) converted	Δ Dimer (mol%) production	Δ Trimer (mol%) production
CM-MgO	4.91	4.91	0.00
MgO(111)	11.41	2.71	7.48
HTC	36.56	6.17	42.73

Table 5. Change in 2-petanone conversion, dimer, and trimer production upon carbon coating.